Ab initio calculations of the phase behavior and subsequent magnetostriction of $Fe_{1-x}Ga_x$ within the disordered local moment picture

George A. Marchant,[1] Christopher D. Woodgate,[1] Christopher E. Patrick,[2] and Julie B. Staunton[1]
[1]*Department of Physics, University of Warwick, Coventry CV4 7AL, United Kingdom*
[2]*Department of Materials, University of Oxford, Oxford OX1 3PH, United Kingdom*

(Received 21 November 2020; revised 29 January 2021; accepted 25 February 2021; published 10 March 2021)

A holistic approach for studying both the nature of atomic order and finite-temperature magnetostrictive behavior in the binary alloy Galfenol ($Fe_{1-x}Ga_x$, $0 \leqslant x \leqslant 0.25$) is presented. The phase behavior is studied via atomistic modeling with inputs from *ab initio* calculations, and the ordered phases of interest at nonstoichiometric concentrations are verified to exhibit $B2$- and $D0_3$-like order. The finite-temperature magnetoelasticity of these phases, in particular the magnetoelastic constant B_1, is obtained within the same *ab initio* framework using disordered local moment theory. Our results provide an explanation for the origin of the experimentally observed peak and subsequent fall in the material's magnetostriction at $x \sim 0.19$, which has been disputed. In addition, we show that it is possible to enhance the magnetostriction of $D0_3$-Fe_3Ga by removing a small fraction of electrons from the system, suggesting that a Fe-Ga-Cu or Fe-Ga-Zn alloy could exhibit greater magnetostrictive properties than Galfenol.

DOI: 10.1103/PhysRevB.103.094414

I. INTRODUCTION

A material property of interest for use in sensor and actuator technologies is magnetostriction, the deformation experienced by a material under the application of an external magnetic field. It provides a means by which to convert between mechanical and electrical energy [1]. In recent decades, the discoveries of materials with exceptional levels of magnetostriction, such as Terfenol-D ($Tb_{1-x}Dy_xFe_2$) [2], have encouraged a research drive toward both the development of magnetostrictive devices [3] and the search for new magnetostrictive materials [4]. A relatively recent development has been the discovery of the iron-based alloys Fe-Ga and Fe-Al (referred to as Galfenol and Alfenol) [5,6]. These materials are fundamentally less magnetostrictive than Terfenol-D, but they remain attractive for applications because they are iron-based, making them relatively inexpensive and mechanically strong [7].

An intriguing and fundamental question to be understood is why adding a small amount (around 20%) of a nonmagnetic element such as Ga can result in such a dramatic increase in magnetostriction (around an order of magnitude greater for Galfenol) compared to pure Fe [5]. Presently, the prevailing theories that describe the origin of this enhancement can be broadly divided into two fundamental mechanisms: intrinsic and extrinsic. The latter theory—established in Refs. [8,9]—attributes the enhancement to the emergence of tetragonal nanoheterogeneities embedded in the (otherwise cubic) lattice. When a magnetic field is applied to the material, these nanoheterogeneities align, resulting in distortion of the entire material along that direction. However, despite there being a number of studies that report the observation of these so-called "nanodomains" [10–12], other reports suggest that their role in Galfenol's magnetostrictive enhancement is relatively insignificant [13,14].

The intrinsic mechanism, on the other hand—which we will be addressing in this study—identifies the enhancement as resulting from the effect that local Ga ordering has on the system's electronic band structure. To describe such a mechanism therefore requires either a fully relativistic treatment of the many-body Schrödinger equation, or a scalar-relativistic treatment augmented by a second-order perturbation theory description of the spin-orbit coupling energy [15]. For a number of years now, calculations of the latter nature have been employed with increasingly large simulation cells to calculate the magnetostriction of ordered phases at particular stoichiometries. These calculations culminated recently with the use of 128-atom supercells to model disordered $Fe_{1-x}Ga_x$ structures, which were determined through *ab initio* calculations of the system's ground-state molecular dynamics [16]. The simulations showed that a peak in magnetostriction occurs at $x = 0.19$, accurately reflecting experimental measurements [5]. Following from a previous study that reported $D0_3$-type ordering to be detrimental to Galfenol's magnetostriction [17], its rapid development around $x = 0.15$ in the molecular dynamics simulations led to the conclusion that it is the origin of the drop in magnetostriction after the peak [16].

An alternative method to the use of supercells is to model compositional disorder with the coherent potential approximation (CPA) [18], which treats disorder via the determination of an effective medium with the same average properties as the disordered system. The CPA was utilized in Ref. [19] to calculate the electronic structure of different "partially ordered" $Fe_{1-x}Ga_x$ phases ($A2$, $B2$, and $D0_3$), however the authors concluded that the use of the CPA could not necessarily

capture Galfenol's magnetostrictive enhancement—if it indeed originates from short-range Ga ordering. Recently, it was demonstrated using the CPA that to homogeneously dope Ga throughout the lattice fails to explain the observed increase in magnetostriction [20]. Nevertheless, calculations of Galfenol's magnetostriction have not yet been carried out on the partially ordered phases where an inhomogeneous CPA [18] is applied.

For completeness, there is also a desire for models of alloys and their properties to take a holistic approach. For example, in the context of *ab initio* calculations, it is desirable to use the description of a material's electronic structure to describe both the nature of the material's compositional order and also subsequent calculations of its physical properties.

Another key challenge to address is the behavior of a material's magnetostrictive properties at finite temperature. In the context of the rare-earth elements, where electrons are highly localized [21], a successful description of finite-temperature magnetoelastic behavior is provided by the single-ion model of Callen and Callen [22–24]. However, the magnetism of Fe originates from itinerant electrons, and it is not unreasonable to expect the single-ion model to fail to capture the relevant physics [25]. To accurately model the temperature dependence of magnetic properties, it is necessary to take into account fluctuations of magnetic degrees of freedom and the subsequent effects of this. A technique that was recently used for the first time to study magnetostriction [20] is the disordered local moment (DLM) picture [26], which is based on the Born-Oppenheimer-like assumption [27] that the timescales of electronic motion and the rearrangement of local magnetic moments are disparate enough that the degrees of freedom of the latter can be considered effectively frozen. It has been demonstrated to be an effective approach to this problem [28–31]. Provided ensemble averages are taken appropriately, this method enables the determination of the temperature dependence of a variety of magnetic properties nonempirically.

In this paper, we first present a description of atomic short-range order in Galfenol based on *ab initio* calculations across a range of temperatures and concentrations of Ga. This approach ensures that any partially ordered, nonstoichiometric phase of $Fe_{1-x}Ga_x$ that we model is compatible with the density functional theory (DFT) description of the bonding in the material provided by its electrons. We identify that the phases of interest are those exhibiting nonstoichiometric $B2$- and $D0_3$-like order. Our calculations show that when Galfenol is annealed below its Curie temperature, the best description of atomic order in the material is given by a nonstoichiometric $D0_3$-like order.

Having identified the phases of interest, we then present *ab initio* calculations of the intrinsic magnetostriction of these phases within the same framework as is used to study the compositional order. These calculations include finite-temperature effects within the DLM picture. The distortion studied is tetragonal [001].

Our calculations show that both the $B2$- and $D0_3$-like nonstoichiometric phases reproduce the experimentally observed increase in magnetostriction with increasing Ga content. Further, the $D0_3$-like phase also successfully reproduces qualitatively the peak and subsequent fall in magnetostriction at $x \sim 0.19$. We attribute this nonmonotonic behavior to the effects of increasing Ga content on the material's band structure.

The rest of this paper is structured as follows. In Sec. II we discuss an atomistic approach for studying compositional order based on *ab initio* calculations. We describe a method for studying the magnetostrictive behavior of partially ordered, nonstoichiometric phases, and we also review our method for calculating the finite-temperature magnetostriction. Then in Sec. III we present the results of our calculations of the atomic order of $Fe_{1-x}Ga_x$ and subsequent results for finite-temperature magnetostriction for the ordered phases of interest. Finally, in Sec. IV we summarize our key findings.

II. THEORY

A. Calculation of compositional order

In this work, we first look to verify that any partially ordered, nonstoichiometric phase of $Fe_{1-x}Ga_x$ that we model is compatible with the DFT description of the bonding in the material provided by its electrons. The composition of a material can be specified by labels $\xi_{i\alpha} \in \{0, 1\}$ to indicate the type of atom occupying the site, so that $\{\xi_{i\alpha}\}$ represents a specific configuration. An ensemble average $\langle \xi_{i\alpha} \rangle = c_{i\alpha}$ gives the probability of a site at $\mathbf{R}_i$ being occupied by an atom of type α in the material. A Gibbs' free energy can be written [26,32–34] for either the paramagnetic or ferromagnetic state of a material in terms of these compositional site-dependent order parameters $\{c_{i\alpha}\}$ and site-dependent chemical potentials $\{\nu_{i\alpha}\}$,

$$F(\{c_{i\alpha}\}) = k_B T \sum_{i,\alpha} c_{i\alpha} \ln c_{i\alpha} - \sum_{i,\alpha} \nu_{i\alpha} c_{i\alpha} + \Omega(\{c_{i\alpha}\}), \quad (1)$$

where the first term describes $-T$ times the configurational entropy $(-T\mathcal{S})$, the second involves chemical potentials to set overall concentrations, and the last, the internal energy Ω, is found by DFT-DLM calculations averaged over compositional configurations, discussed below. The $\{\nu_{i\alpha}\}$ have a site dependence for the purposes of evaluating the linear-response *ab initio*, which is discussed in detail in Ref. [34]. The paramagnetic or ferromagnetic state is appropriate depending on whether the temperatures at which atomic ordering and material annealing take place are higher or lower than the material's Curie temperature.

One can find the nature of the infinitesimal composition fluctuations to which the high temperature, high configurational entropy state (A2 phase) of the material is unstable from an expansion of the free energy and a linear stability analysis [26,32–34]. Whether atoms of particular elements preferentially segregate onto certain sublattices, order into longer period patterns, and the temperature below which such a compositional rearranging mode is stable can be determined. Moreover, the second-order derivatives of DFT-DLM energy

$$S^{(2)}_{i\alpha;j\alpha'} = \frac{\partial^2 \Omega}{\partial c_{i\alpha} \partial c_{j\alpha'}}$$

can be interpreted as atom-atom interchange parameters for use in further atomistic modeling.

For a two-species alloy such as $Fe_{1-x}Ga_x$, the state of the system is specified by one independent occupation number

on each site, and we have that $\xi_{iB} = 1 - \xi_{iA}$. As there is only one independent variable on each site, we drop species labels α, α', A, B. The ensemble average of a site occupancy is denoted by $\langle \xi_i \rangle = c_i$, and it is these sitewise concentrations that are used in our *ab initio* calculations of magnetic torque and magnetostriction.

To determine a self-consistent set of sitewise concentrations at a given temperature and overall gallium concentration, we take the *ab initio* calculations of $S^{(2)}_{i;j}$ to fit the interchange parameters V_{ij} of a Bragg-Williams Hamiltonian representing the internal energy, of the form

$$\mathcal{H}(\{\xi_i\}) = \frac{1}{2}\sum_{i,j} V_{ij}\,\xi_i\xi_j + \mu \sum_i \xi_i, \tag{2}$$

where $V_{ij} = (V_{AA} + V_{BB} - 2V_{AB})_{ij}$, as is the convention [35]. Either Fe or Ga can be chosen as the "host" species, but of course all results must be host-independent. As is the case in the DFT-DLM calculations, we assume here that the distribution is uncorrelated, allowing us to evaluate the internal energy of the system as $\langle \mathcal{H}(\{\xi_i\}) \rangle = \Omega\{c_i\}$.

Working in the canonical ensemble with fixed overall concentration $c = \sum_i c_i$, we are free to set the chemical potential term to zero, and we write the free energy of the system as

$$F = k_B T \sum_i c_i \ln c_i + (1 - c_i)\ln(1 - c_i) + \frac{1}{2}\sum_{i,j} V_{ij}\,c_i c_j. \tag{3}$$

To compute the ground-state concentrations, we use a concentration-preserving gradient descent in the manner of Chen and Khachaturayan [36]. This can be thought of as simulating diffusion across the lattice, but for our purposes we neglect constants associated with characteristic timescales and instead look for the steady state (i.e., self-consistent) solution. Formally, we solve

$$\frac{dc_i}{dt} = \sum_j L_{ij}\frac{\partial F}{\partial c_j}, \tag{4}$$

where

$$L_{ij} = \begin{cases} -N_{\text{nn}}, & i = j, \\ 1, & i,\, j \text{ nearest neighbors}, \\ 0, & \text{otherwise}, \end{cases} \tag{5}$$

to preserve overall concentration. ($N_{\text{nn}} = 8$ in the case of the bcc lattice.) We interpret a steady-state solution, $\frac{dc_i}{dt} = 0$, as the ground-state configuration of the system for which the free energy is minimized.

We also look to verify the results obtained by the diffusive method via Monte Carlo simulations of the system based on the atomic site occupancies, $\xi_{i\alpha}$. The algorithm is an adaptation of the usual Metropolis Monte Carlo algorithm, which conserves overall concentrations of each species [37]. A pair of sites on the lattice is picked at random, and it is considered what the change in energy, $\Delta\mathcal{H}$, would be if the two site occupancies were swapped. If the change is negative, the move is accepted. If the change is positive, the move is accepted with probability $P = \exp(-\beta\,\Delta\mathcal{H})$. The algorithm is described in more detail in Ref. [38].

B. Modelling of nonstoichiometric phases

To efficiently model *ab initio* the magnetostriction of the computed phases at nonstoichiometric concentrations, we have utilized the CPA within DFT to describe the movement of electrons through these compositional arrangements [39]. The CPA, implemented here via Korringa-Kohn-Rostoker multiple-scattering theory (KKR-MST) [40], models the effect of atomic disorder at a given site using a mean-field description, wherein a coherent medium is determined that reflects the average behavior of the disordered system. Central to the construction of this self-consistent effective medium is the CPA condition, which states that the embedding of an impurity with the average properties of the effective medium must leave the properties of that medium unchanged.

This is the same framework that allows us to implement a linear-response analysis to determine the atomic short-range order that is prevalent in both paramagnetic and ferromagnetic $Fe_{1-x}Ga_x$ high-temperature bcc solid solutions. In this way, we set up a holistic approach to describe both magnetostriction and atomic arrangements from the same fundamental model of the interacting electrons of Fe-Ga alloys.

In our previous study on the magnetostriction of the A2 phase of $Fe_{1-x}Ga_x$, we applied the CPA equally on all lattice sites, reflecting that phase's complete chemical disorder. We now wish to study nonstoichiometric concentrations of ordered and partially ordered structures, so we opt to describe the partial order of these phases using a scheme previously demonstrated by Pindor *et al.* [41] and Khmelevska and Khmelevsky [19], in which the CPA is selectively applied at sites that in the stoichiometric phase would be occupied by Ga. We validate these models of the atomic arrangements in the partially ordered and nonstoichiometric phases using our *ab initio* atom-atom interchange parameters in further atomistic simulations.

Figure 1 shows the possible partially ordered phases of interest pictorially, where we have included the fully disordered $A2$ phase for the sake of comparison. Note that the occupancy of the Ga sites is chosen such that the total Ga concentration x is conserved. In the $B2$-like phase, for example, the concentration at the Ga site is $2x$ to account for its absence on the other site. We also note the Wyckoff labels given in parentheses beside each of the atomic formulas, which will be used in this paper to distinguish inequivalent sites in the unit cell.

C. Definition of magnetoelasticity

In this study, we will be employing the linear magnetoelastic coupling model of intrinsic magnetostriction, which we describe in greater detail in Ref. [20]. In brief, the model describes magnetostriction as an outcome of the response of a magnetic crystal's magnetocrystalline anisotropy (MCA) to structural distortions described by the strain tensor ε_{ij}. In cubic structures this magnetoelastic energy is given by

$$\begin{aligned} E_{\text{me}} = {} & B_1\left(\alpha_x^2\varepsilon_{xx} + \alpha_y^2\varepsilon_{yy} + \alpha_z^2\varepsilon_{zz}\right) \\ & + B_2(\alpha_x\alpha_y\varepsilon_{xy} + \alpha_y\alpha_z\varepsilon_{yz} + \alpha_z\alpha_x\varepsilon_{zx}), \end{aligned} \tag{6}$$

where α_i are the components of the magnetization direction's unit vector with respect to the crystallographic axes, implying

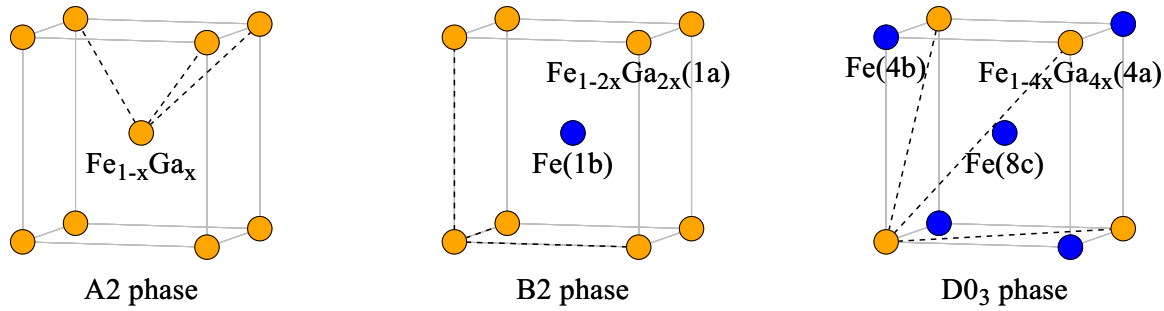

FIG. 1. Diagrams of the nonstoichiometric $A2$, $B2$-like, and $D0_3$-like phases of $Fe_{1-x}Ga_x$. Dashed lines denote unit vectors. In the $D0_3$ case, we have opted to show only one of the two 8c sites.

that the MCA picks up lower-symmetry terms when the crystal is strained which are characterized by the magnetoelastic constants B_1 and B_2 [42]. The energy saved by this strain must necessarily be limited by the crystal's elastic energy,

$$E_{\text{el}} = \tfrac{1}{2}c_{11}\left(\varepsilon_{xx}^2+\varepsilon_{yy}^2+\varepsilon_{zz}^2\right)+\tfrac{1}{2}c_{44}\left(\varepsilon_{xy}^2+\varepsilon_{yz}^2+\varepsilon_{zx}^2\right) + c_{12}(\varepsilon_{xx}\varepsilon_{yy}+\varepsilon_{yy}\varepsilon_{zz}+\varepsilon_{zz}\varepsilon_{xx}), \tag{7}$$

itself characterized by the elastic constants c_{ij}. It is thus by determining the strain at which these energies are balanced that we can derive expressions for the cubic magnetostriction constants,

$$\lambda_{001} = -\frac{2}{3}\frac{B_1}{c_{11}-c_{12}} \quad \text{and} \quad \lambda_{111} = -\frac{1}{3}\frac{B_2}{c_{44}}. \tag{8}$$

In this study, however, we will be focusing solely on the tetragonal magnetostriction constant λ_{001}, primarily due it being the parameter of interest when discussing Galfenol's magnetostrictive enhancement [43].

To calculate B_1, we utilize the torque method set out by Wang *et al.* [44], in which we measure the linear response of the azimuthal component of the magnetic torque, $T_\theta = -\partial E/\partial\theta$, to small distortions of the lattice along the z axis. We therefore perform a least-squares fitting according to the expression

$$T_{\theta=45^\circ} = B_1\varepsilon_{zz}, \tag{9}$$

which can be straightforwardly derived by taking the azimuthal derivative of Eq. (6).

D. Disordered local moment theory and the calculation of magnetic torque

The magnetic torque in Eq. (9) is calculated from first principles within the disordered local moment picture [26]. In short, DLM theory describes magnetic materials at finite temperature as an ensemble of thermally disordered local moments with orientational degrees of freedom $\{\hat{e}_i\}$. Each local moment is self-consistently maintained by a local Weiss field $\boldsymbol{h}_i$, in that each field simultaneously dictates and is dictated by the system's rapid-timescale electron dynamics. The probability distributions $P_i^0(\hat{\boldsymbol{e}}_i)$ of these moment orientations are predetermined by the choice of the temperature-dependent parameter $\boldsymbol{\lambda}_i = \boldsymbol{h}_i/k_{\text{B}}T$, meaning that the temperature T associated with a given probability distribution is ascertained by calculating the size of the local Weiss field. Naturally, the sizes of the local order parameters $\boldsymbol{m}_i$ are provided by taking the weighted average of the moment orientations at each site, leading to the compact expression

$$m_i = \coth(\lambda_i) - \frac{1}{\lambda_i}, \tag{10}$$

from which we also have the average magnetic order parameter

$$m = \frac{\sum_i m_i\mu_i}{\sum\mu_i} \tag{11}$$

in terms of the magnitudes of each site's magnetic moment, $\{\mu_i\}$ [26].

Crucially, the explicit dependence of the DLM model's free energy on $\{P_i^0(\hat{\boldsymbol{e}}_i)\}$ provides a natural solution for the magnetic torque at each lattice site in terms of partial averages of the grand potential $\langle\Omega\rangle_{\hat{\boldsymbol{e}}_i}$,

$$T_{\theta,i} = -\frac{\partial}{\partial\theta}\left(\int P_i^0(\hat{\boldsymbol{e}}_i)\langle\Omega\rangle_{\hat{\boldsymbol{e}}_i}d\hat{\boldsymbol{e}}_i\right), \tag{12}$$

where the grand potential is calculated using solutions to the fully relativistic Dirac-Kohn Sham equations [29]. Thus, while the primary strength of the model is its treatment of magnetism at finite temperature, it also allows us to resolve each unique atom's contribution to the total magnetoelasticity. In the case of B_1, these contributions are defined by

$$T_{\theta=45^\circ,i} = B_{1,i}\varepsilon_{zz}. \tag{13}$$

We are therefore able to evaluate the influence of the atoms' local environments on the material's magnetostriction. It is important to stress, however, that different values of magnetoelasticity at different sites do not necessarily imply the existence of internal strains. The site resolution should only be considered a gauge of the extent to which each atom contributes to the total magnetoelasticity.

A more complete description of the torque method in the context of DLM theory can be found in Ref. [29], while more details on the procedure for calculating the magnetoelastic constants within DLM theory can be found in Ref. [20].

E. Second-order perturbation theory of magnetocrystalline anisotropy

While the implementation of the torque method within DLM theory allows for the calculation of MCA and magnetoelasticity from first principles, the calculations do not

necessarily reveal the exact nature of the spin-orbit interactions from which these phenomena originate. It is therefore necessary to consider spin-orbit coupling in a form that will give us insight into the key interactions in order to interpret the *ab initio* calculations of B_1 provided by DLM theory. With that in mind, the lowest-order perturbative contribution of the spin-orbit coupling Hamiltonian H_{SOC} to the MCA is

$$E_{\mathrm{MCA}} = (\xi^2) \sum_{o,u} \frac{\langle o|L_z|u\rangle^2 - \langle o|L_x|u\rangle^2}{E_o - E_u}, \tag{14}$$

where L_i are components of the orbital momentum operator, ξ is the spin-orbit coupling constant, and o and u refer to occupied and unoccupied states [45]. We can better relate this expression for the MCA to the magnetoelastic constant B_1 by taking the first derivative of the strain-dependent MCA in the cubic configuration, giving

$$B_1 = \left.\frac{\partial E_{\mathrm{MCA}}}{\partial \varepsilon_{zz}}\right|_{\varepsilon_{zz}=0}. \tag{15}$$

This shows that the enhancement of B_1 relies upon increasing the response of the difference between $\langle o|L_z|u\rangle^2$ and $\langle o|L_x|u\rangle^2$ to structural distortions along the z-axis (assuming that ξ remains constant). The denominator in Eq. (14) suggests that states in the immediate vicinity of the Fermi level are those that should be focused on. In addition, Ref. [45] tells us that the only nonzero matrix elements among the d orbitals—which should of course contribute the most to E_{MCA}—are

$$\langle xz|L_z|yz\rangle = 1, \quad \langle x^2 - y^2|L_z|xy\rangle = 2, \quad \langle xy|L_x|xz, yz\rangle = 1,$$
$$\langle x^2 - y^2|L_x|xz, yz\rangle = 1, \quad \langle z^2|L_x|xz, yz\rangle = \sqrt{3}. \tag{16}$$

If we therefore apply a positive strain along the z-axis, the enhancement of L_z elements and/or the diminishing of the L_x elements will provide a positive value of magnetostriction. It is especially important to note that the terms in Eq. (16) only apply to states belonging to the same spin channel. To account for coupled states belonging to opposite spin channels, one must exchange L_x and L_z in each expression, for example

$$\langle xz|L_z|yz\rangle = 1 \rightarrow \langle xz|L_x|yz\rangle = 1. \tag{17}$$

We emphasize that our use of second-order perturbation theory in this study is part of a qualitative analysis of the *ab initio* results provided by our method's solving of the fully relativistic Dirac-Kohn Sham equations [29]. This is in contrast to its previous use as a method for calculating magnetoelasticity directly [15,17,44–47].

For more computational details regarding the calculation of magnetoelasticity and density of states, including specific details on Brillouin zone integration and angular momentum truncation, please see Ref. [20].

III. RESULTS AND DISCUSSION

A. Compositional order

Calculations for the gradient-based approach were performed using a code developed in-house which solves Eq. (4) using a simple forward Euler method until a steady-state solution is reached. Initial conditions are chosen to be a homogeneous state with a small amount of random noise. The system simulated consisted of 128 lattice sites with periodic boundary conditions. Results at 5%, 10%, 15%, 20%, and 25% Ga were verified on a system of 1024 lattice sites, with no discernible difference in the computed structure between the small and large systems, ensuring we avoided issues associated with finite-size effects. We sampled two indicative temperatures, 800 and 1200 K, for which the system is in a ferromagnetic and paramagnetic state, respectively.

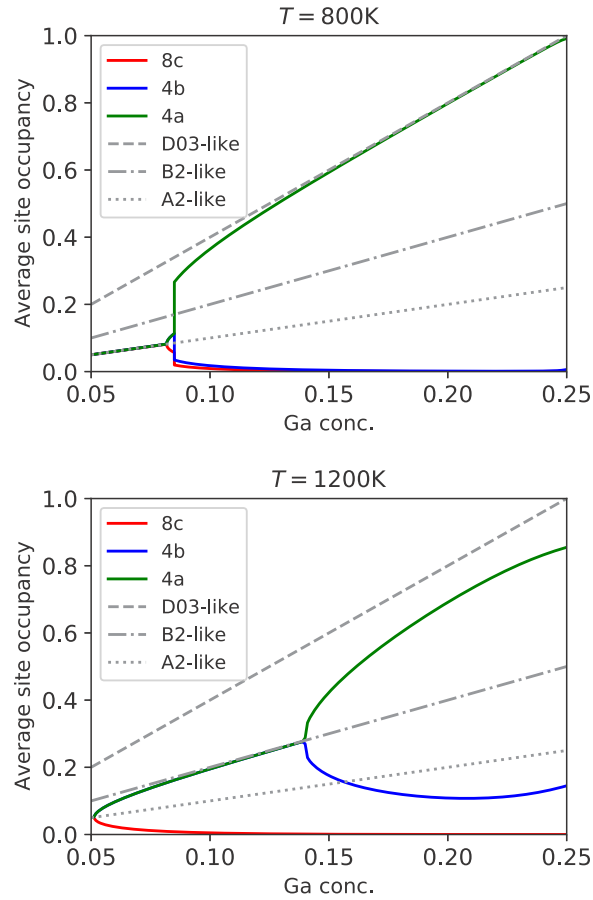

FIG. 2. Computed site occupancies at 1200 and 800 K. The three dashed lines are indicative of what site occupancies would be in a pure $A2$ phase, what 4a and 4b sites would be in a pure $B2$-like phase, and what 4a site occupancies would be in a pure $D0_3$-like phase. At low concentrations of gallium, the system is in an $A2$ state, with the Ga spread homogeneously across the lattice. At 1200 K the system first transitions to $B2$-like order before further transitioning to a mixed $B2$-$D0_3$ state at approximately 14% Ga. At 800 K the transition is much sharper, and the system transitions to an almost pure $D0_3$-like state at approximately 8% Ga.

For the Galfenol system in a ferromagnetic state, we compute $V_{ij} = 0.014$ Ry for nearest neighbors and $V_{ij} = 0.008$ Ry for next-nearest neighbors, with all others set to zero. In the paramagnetic state, we compute these values as 0.023 and 0.006 Ry, respectively. It should be highlighted that in the ferromagnetic state, the relative strength of the second-nearest-neighbor interaction is large compared with the paramagnetic state.

Computed concentrations at both temperatures are shown in Fig. 2. We find that the system can be completely classified

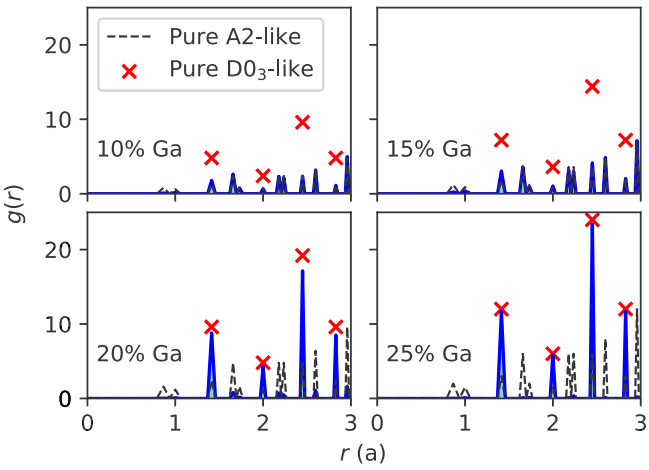

FIG. 3. Average radial Ga-Ga densities for Galfenol obtained via Monte Carlo simulations. The interchange parameters used were those computed for the ferromagnetic state, and the simulation temperature was 800 K. The black dashed lines indicate the expected radial density for a completely disordered ($A2$) state, while the red crosses indicate the expected peaks for $D0_3$-like order.

in terms of occupancies of the sites specified in the $D0_3$ structure (which implicitly contains the $B2$ and $A2$ structures). It can be clearly seen that for the region of interest ($x \sim 0.2$) the system is in a $D0_3$-like state. For 800 K the state is very pure, while the results at 1200 K are suggestive of a $B2$-like state heavily modulated by $D0_3$-type order. We associate this with both a higher level of thermal disorder and also the comparative weakness of the second-nearest-neighbor interaction for the system in the paramagnetic state. Further calculations were performed at 1600 K, and at this temperature we find that the observed order is almost purely $B2$-like.

These results are in good agreement with existing literature, which suggests that samples annealed at high temperature exhibit $B2$-like order, while samples annealed at lower temperatures tend toward $D0_3$-like order. This serves to validate our choice of nonstoichiometric phases on which to perform calculations.

We also performed atomistic Monte Carlo simulations of the system, and we extracted pairwise correlations from equilibrium configurations. In the case of Galfenol, it is sufficient to consider Ga-Ga correlations to classify the nature of observed order. Figure 3 shows plots of the Ga-Ga radial density for an equilibrated system consisting of 8192 lattice sites with periodic boundary conditions, at a simulation temperature of 800 K (below the Curie temperature). The results show good agreement with the diffusion-based approach, and clearly demonstrate the emergence of $D0_3$-like order with increasing Ga concentration.

From these results we conclude that the two ordered phases of interest are the $D0_3$ and $B2$ phases.

B. Magnetoelasticity of partially ordered phases

1. B2 phase

We begin by calculating the magnetoelastic composition dependence of the nonstoichiometric $B2$ phase of $Fe_{1-x}Ga_x$

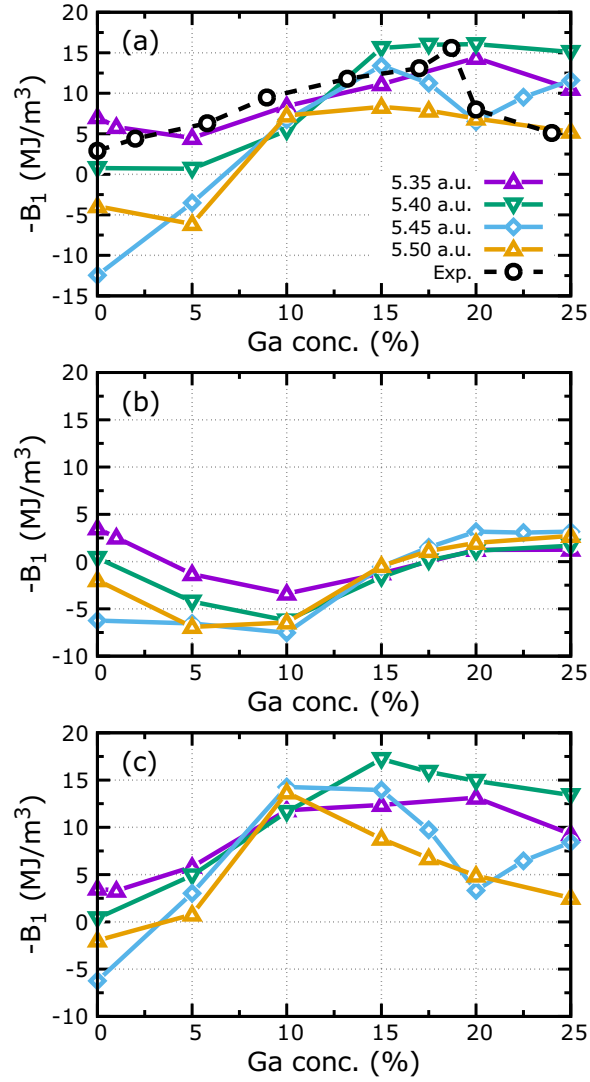

FIG. 4. Total and site-resolved values of the magnetoelastic constant $-B_1$ as a function of Ga content in nonstoichiometric $B2$ $Fe_{1-x}Ga_x$ for lattice parameters between 5.35 and 5.50 a.u. (a) $-B_1$ for the total system and experimental measurements at room temperature [5]; (b) site-resolved $-B_1$ at site 1a (see Fig. 1); (c) site 1b.

($0 < x < 0.2$) over a range of lattice parameters, $a = 5.35$–5.50 a.u. (at low temperatures, the experimental value of $a = 5.40$ a.u.). The results of these calculations can be found in Fig. 4, in which we have included the site-resolved values of $-B_1$ (negative so that its sign is that of λ_{001}). Experimental values of $-B_1$ have also been included by using the data for λ_{001}, c_{11}, and c_{12} in Ref. [5] and rearranging Eq. (8).

Focusing on the total magnetoelasticity for now, we first note the significant magnetoelastic volume dependence of pure Fe—a result that was previously found in Ref. [20]—where the expansion of the lattice leads to $-B_1$ changing in sign from positive to negative. As Ga is added to the 1a site up to around 15%, there is a consistent increase in magnetoelasticity across all lattice parameters up to between ∼7 and 15 MJ/m^3, including a change in sign for $a = 5.45$ and 5.50 a.u. For concentrations greater than 15–20 % the magnetoelasticity tends to slightly decrease, though the compositional

behavior here could mostly be described as relatively benign in comparison to that seen at lower concentrations. The exception is when $a = 5.45$ a.u. for which a local minimum occurs at 20% Ga content as the magnetoelasticity quite rapidly decreases and then increases again. We also observe that when $x = 0.25$ and $a = 5.50$ a.u., then $-B_1 \sim 5$ MJ/m^3, which is notably small compared to the values at smaller volumes, which range between ∼10 and 15 MJ/m^3.

If we now consider the contribution to the magnetoelasticity from each lattice site, where the site 1a denotes the doped site and 1b denotes the pure Fe site, the difference between the two is immediately obvious. While the 1b site demonstrates a significant decrease in magnetoelastic volume dependence, with each isovolumetric curve converging toward values of ∼2–3 MJ/m^3, the 1a site on the other hand accounts almost entirely for the total magnetoelastic enhancement. The resolution between atomic sites also reveals a more consistent magnitude in the peaks of $-B_1$ for each volume, while the location of the peak is shifted downward with respect to Ga content as the lattice expands. This means that the size of the peak for the larger volumes is limited due to the significant negative contribution to the magnetoelasticity from the 1a site at lower concentrations.

2. *D03-like phase*

We move on now to our calculations of magnetoelasticity in the $D0_3$-like phase, the results of which are plotted in Fig. 5. It is immediately obvious that it leads to a much greater enhancement in magnetoelasticity than that seen in the $B2$ phase, reaching peaks of $-B_1 \sim 35$ MJ/m^3 for $a = 5.45$ a.u.—over twice the experimentally measured peak. The qualitative behavior of the isovolumetric curves tells a similar story to the $B2$ phase, however, demonstrating a consistent increase in $-B_1$ up to ∼15% Ga content followed by a moderate decrease, which is less than that seen in the experimental data. An exception to this trend is the behavior of the system when $a = 5.50$ a.u. at Ga concentrations above 20%, where we see a sudden increase in $-B_1$. Observations based on the site-resolved magnetoelasticity are also familiar. Namely, the dominance of the 8c sites reflects that of the 1b site in the $B2$-like phase, due to the fact that they are the only sites whose nearest neighbors are affected by the selective doping. The 4a and 4b sites meanwhile act as the counterparts to the $B2$-like phase's 1a site, showing an initial decrease in $-B_1$ that counterbalances the magnetoelastic enhancement on the 8c site, and then a clear suppression of the volume dependence as the Ga content increases further.

3. *Comparisons between the partially ordered phases*

Thus far we have seen that, in both the $B2$- and $D0_3$-like phases, there is a consistent increase in magnetoelasticity when between 10% and 15% Ga is doped into the system, across a significant range of lattice volumes. Based on site-resolved calculations, this enhancement is driven primarily by the 1b and 8c sites for the $B2$- and $D0_3$-like phases, respectively, which Fig. 1 shows are the only sites whose nearest neighbors change as Ga is added. In the $B2$-like phase, all eight nearest neighbors change, while in the $D0_3$-like phase only four sites—at the vertices of tetrahedra—change.

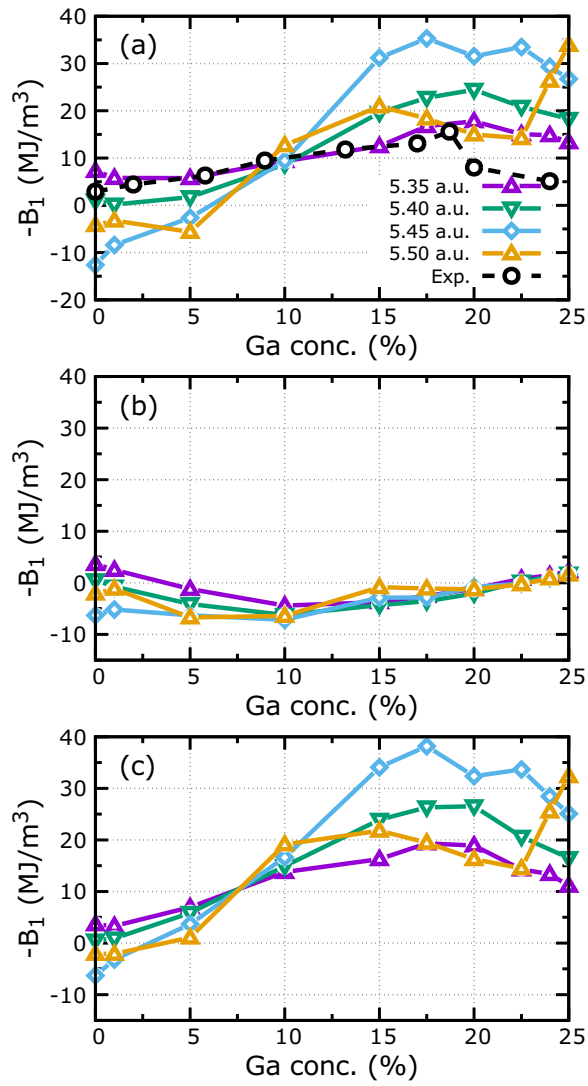

FIG. 5. Total and site-resolved values of the magnetoelastic constant $-B_1$ as a function of Ga content in nonstoichiometric $D0_3$-like $Fe_{1-x}Ga_x$ for lattice parameters between 5.35 and 5.50 a.u. (a) $-B_1$ for the total system and experimental measurements at room temperature [5]; (b) combined contribution from sites 4a and 4b (see Fig. 1); (c) combined contribution of the two 8c sites.

Figure 6 shows that at small x the 1b and 8c sites are almost equivalent in terms of their magnetoelastic concentration dependence, suggesting that the leading contribution to the magnetoelasticity at these concentrations is simply the average number of Fe nearest neighbors, which is equivalent for these sites. At concentrations greater than ∼10%, the behaviors of the two sites diverge, with the magnetoelasticity of the 8c site continuing to increase while the 1b site's evolution is comparatively flat. The enhancement at $a = 5.45$ a.u. is especially profound, with $-B_1$ reaching values over twice as large as those seen in experimental measurements [5]. A notable anomaly in terms of concentration dependence can be seen when $a = 5.50$ a.u., at around $0.225 < x < 0.25$, where we see a sudden increase in magnetoelasticity after the initial peak. While this unusual feature is interesting in and of itself, its corresponding lattice parameter is greater than the exper-

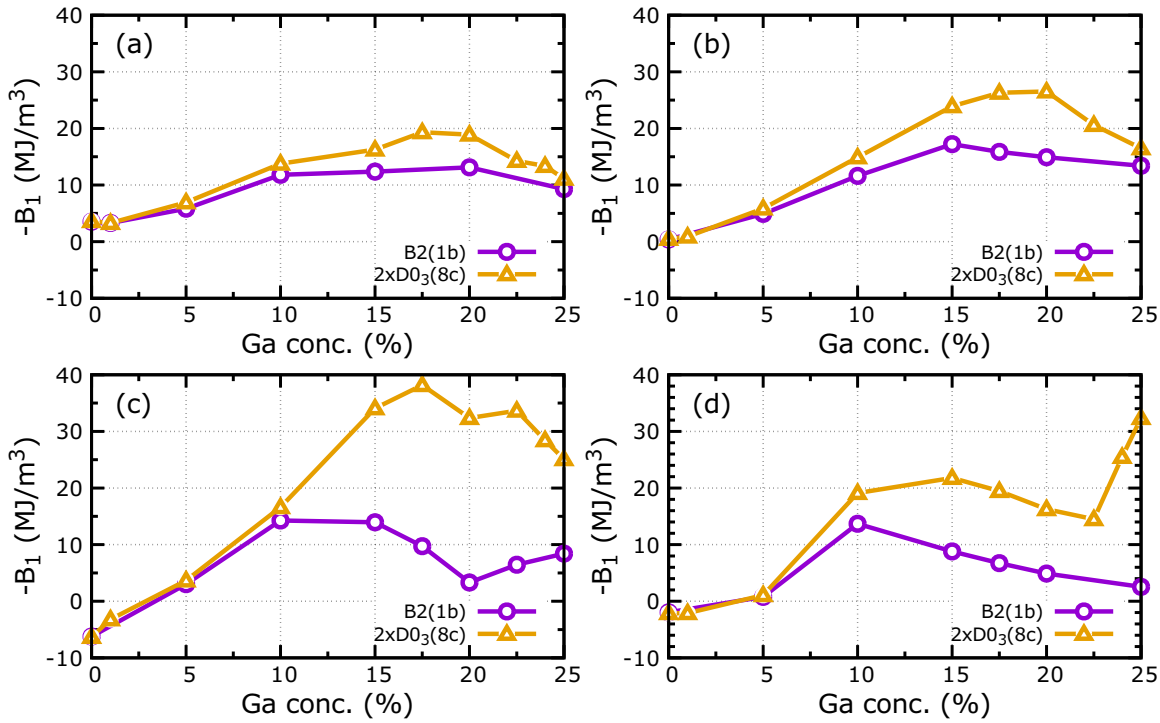

FIG. 6. Comparisons of the site-resolved magnetoelastic Ga concentration dependence at sites 1b in the $B2$-like phase and 8c in the $D0_3$-like phase, for different lattice parameters: (a) 5.35 a.u., (b) 5.40 a.u., (c) 5.45 a.u., and (d) 5.50 a.u.

imentally measured values of Galfenol. We therefore opt not to consider its origin any further, but we present it here as a curiosity.

In summary, though the behavior beyond 10% Ga content in both phases is highly volume-dependent, our calculations show quite clearly that homogeneously replacing some number of Fe's nearest neighbors with Ga in a cubic configuration enhances magnetoelasticity.

4. Comparisons to previous studies

In sharp contrast with previous findings [17,48] and the insights made by subsequent investigations that have been informed by those findings [16,19,49], our calculations consistently show that the $D0_3$-like phase is *not* detrimental to the magnetostriction of Galfenol and even exhibits magnetoelasticity that is more than twice that of the experimentally measured peak. Not only that, but the $B2$-like phase alone is able to account for the experimentally observed enhancement in magnetoelasticity, despite the results of Kumagai *et al.* [48] suggesting that the $A2$ phase has the largest magnetoelasticity among it, $B2$, and $D0_3$. It should be noted, however, that these results are not necessarily in conflict with the more recent results of Wang *et al.*, whose optimized superlattice calculations found large amounts of $D0_3$-type order at Ga concentrations of $\sim$15% and above. Their conclusion was that this ordering limits the growth of the magnetoelasticity and causes its decrease after the peak, whereas our results suggest that the onset of $B2$- and $D0_3$-like ordering is necessary for enhancement.

To gain some insight as to the electronic origin of this enhancement, in the following sections we will analyze the density of states of these phases, with a particular focus on the 1b and 8c sites due to their dominating contribution to the magnetoelastic concentration dependence.

C. Density of states and band-filling analysis

1. B2-like phase

To begin our analysis of the $B2$-like phase's band structure, we have calculated the density of states (DOS) of the 1b site—that which accounts solely for the magnetoelastic enhancement—in $Fe_{1-x}Ga_x$ for Ga concentrations of 0%, 15%, and 25%, and we plotted the results in Fig. 7. For these calculations, as well as the calculations used in the band-filling analysis that appear later in this section, the unit-cell volume is fixed so that $a = 5.45$ a.u., i.e., the experimentally measured lattice parameter for $Fe_{0.85}Ga_{0.15}$ [50].

The most obvious change we see as Ga is added to the system is the growth of a large peak in the minority channel of the DOS, emerging at low Ga concentrations from above the Fermi level before centralizing around the Fermi level when Ga content reaches 25%. From the peak's location relative to the d bands as a whole—it being around their energetic "center of mass" so to speak—we can infer that the peak is generally made up of nonbonding states [51]. This is consistent with the physical picture, in which the effect of increasing Ga content in the $B2$-like phase is to replace some proportion of all nearest neighbors to the 1b site with Ga's p orbitals. The tight-binding model [51] then tells us that the strengthening of that site's nonbonding characteristics is due to the weakness of pd-type bonding for that particular nearest-neighbor symmetry.

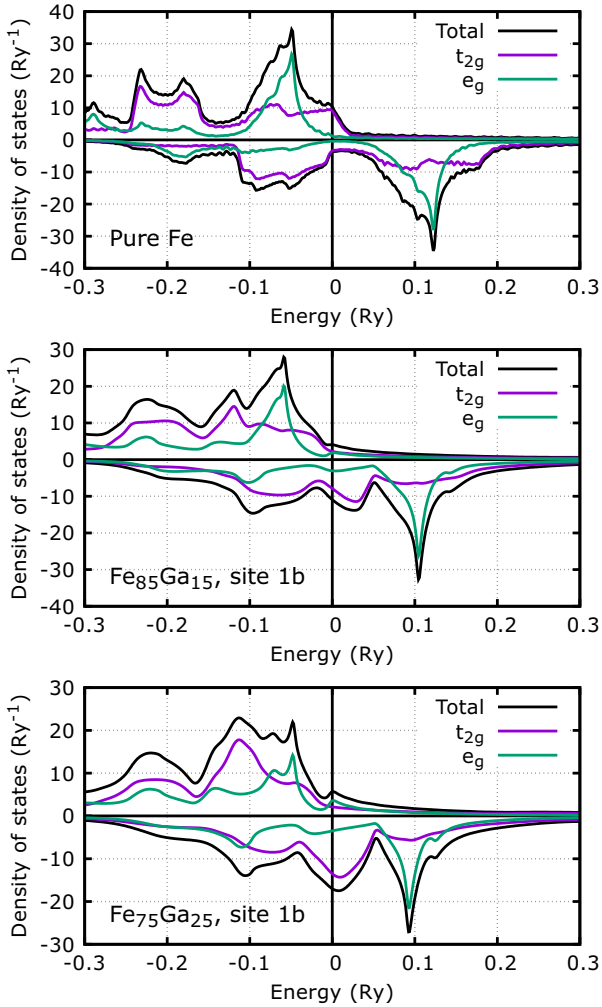

FIG. 7. The scalar-relativistic density of states of $Fe_{1-x}Ga_x$ in the $B2$-like phase ($x = 0$, 0.15, and 0.25) at the 1b site, where zero energy is defined to be the Fermi energy. Also shown are the orbital-resolved density of states, separated into e_g and t_{2g} states.

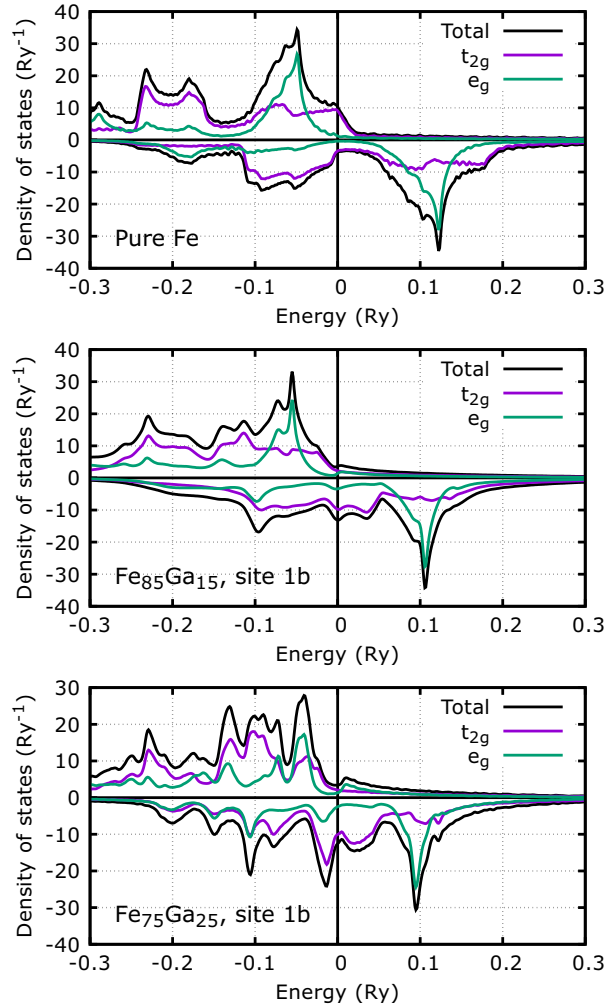

FIG. 8. The scalar-relativistic density of states of $Fe_{1-x}Ga_x$ in the $D0_3$-like phase ($x = 0$, 0.15, and 0.25) at the 8c site in the $D0_3$ phase, where zero energy is defined to be the Fermi energy. Also shown are the orbital-resolved density of states, separated into e_g and t_{2g} states.

By projecting the DOS onto the t_{2g} (xy, yz, and xz) and e_g (z^2, $x^2 - y^2$) orbitals, it becomes clear that the emergence of this peak derives primarily from the t_{2g} orbitals. Once again this follows from the physical picture, which shows that the bonding between t_{2g} orbitals is notably stronger than e_g orbitals in bcc Fe due to their much greater overlap, suggesting that the weakening of this bonding from the insertion of Ga will mostly lead to changes in the t_{2g}-projected DOS.

2. D03-like phase

Calculations of the total and orbital-resolved DOS on the 8c site of $Fe_{1-x}Ga_x$ in its nonstoichiometric $D0_3$-like phase (where $x = 0$, 0.15, and 0.25) can be found in Fig. 8. There are clear parallels between these results and those of the $B2$-like phase, the primary one being the appearance of a peaklike feature above the Fermi energy in the minority DOS at lower Ga concentrations, which shifts downward in energy and grows in size as more Ga is added. A key difference, however—which becomes more obvious as Ga content increases—is that this feature is now made up of two distinct peaks, with the one at lower energy being almost twice as large when there is 25% Ga. From the orbital-projected DOS of $Fe_{75}Ga_{25}$, we observe some additional features in the e_g states, including small peaks in the minority and majority DOS just below and above the Fermi level, respectively. Referring back to the DOS for the $B2$-like phase, we find that these small peaks also appear but are less prominent. Before we probe the effects of these various features in the DOS on the magnetoelasticity of the material, we will provide a qualitative analysis of their electronic origin using the tight-binding model [51].

3. Tight-binding analysis of the density of states

Here we will focus on the large peaks that appear in the minority DOS around the Fermi level as Ga concentration is increased, in particular the origin of the apparent "splitting" of the peak that occurs when going from the $B2$-like phase to the $D0_3$-like phase.

Intuitively, this occurrence can be understood as a band splitting due to the increased order of the $D0_3$ phase, bearing in mind that Fe_3Ga is stoichiometric in the $D0_3$-like phase and

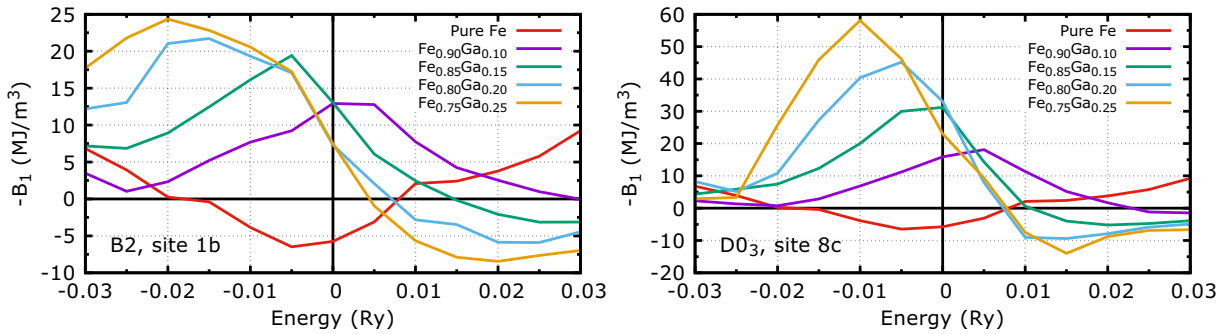

FIG. 9. Calculated Fermi level dependence of the site-resolved MCA in tetragonally deformed ($\varepsilon_{zz} = 0.2\%$) $Fe_{1-x}Ga_x$ ($x = 0$, 0.10, 0.15, 0.20, and 0.25) for the 1b site of the $B2$ phase (left) and the 8c site of the $D0_3$ phase (right).

nonstoichiometric in the $B2$. It follows then that the nonstoichiometric $B2$-like phase of Fe_3Ga, which can be understood as a radially averaged approximation of the stoichiometric $D0_3$ phase, would exhibit a feature in its DOS that is essentially an average of the $D0_3$'s more ordered band structure.

For a more robust explanation, however, we will make use of the Slater-Koster tight-binding model, which describes the interaction between orbitals in terms of their overlap [51]. To simplify the analysis, we will focus on the following two bonding energy terms:

$$E^{\sigma}_{xy-xy} \propto \beta_x^2\beta_y^2 V^{\sigma}, \quad E^{\sigma}_{x-yz} \propto \sqrt{3}\beta_x\beta_y\beta_z V^{\sigma}, \qquad (18)$$

which describe σ-type bonding of strength V^{σ} between orbitals that are separated by the unit vector $\hat{\beta}$, where the interaction is between xy-xy (d-d/Fe-Fe) orbitals and x-yz (p-d/Ga-Fe) orbitals, respectively. Referring back to Fig. 1, to calculate the total nearest-neighbor bonding energy for the 1b and 8c site we need only sum the contributions from each nearest neighbor. By performing these sums, it becomes clear that the fourth-order angular dependence of the xy-xy term (as with the other d-d terms) ensures that the nearest-neighbor bonding energy is equivalent for both the 1b and 8c sites, assuming that disordered sites can be treated by linearly combining the contribution from each atomic species. However, the third-order angular dependence of the x-yz term (again consistent with other p-d terms) leads to a nonzero energy for the 8c site and zero for the 1b site, thus distinguishing their bonding energies. This qualitative analysis tells us that the splitting of the peak in the minority DOS of the $D0_3$-like phase is an outcome of pd-type bonding, rather than dd-type.

Now that we have some understanding of the bonding origins of the peaks in the minority channel of the DOS around the Fermi level, we will investigate their influence on the magnetoelasticity of these phases by studying its dependence on the location of the Fermi level.

4. Band-filling analysis of magnetoelasticity

An effective way of probing the effect of particular features in the DOS on spin-orbit phenomena—such as MCA and magnetoelasticity—is to artificially vary the Fermi energy and determine the response of said phenomena [52]. For this purpose, we have opted to calculate the Fermi level dependence of Galfenol's magnetoelasticity. Figure 9 shows a comparison of the magnetoelastic Fermi-level dependence in the $B2$- and $D0_3$-like phases of $Fe_{1-x}Ga_x$ (more specifically, sites 1b and 8c) over a range of Ga concentrations ($x = 0.1$–0.25), as well as bcc Fe.

Note that our calculations for bcc Fe show a negative magnetostriction, which according to experiment should be the wrong sign [5]. This is due to the choice of lattice parameter, which means that the bcc Fe lattice has been expanded by 0.05 a.u. relative to experimentally measured lattice parameters. These results are therefore consistent with Ref. [20], in which our calculations suggest that Fe has a positive magnetostriction when using experimental lattice parameters and that an expansion of 0.05 a.u. causes the magnetostriction to become negative. They are also consistent with experimental results, which show that the contraction of the Fe lattice leads to an increase in magnetostriction [53]. For more details on the volume dependence of Fe's magnetostriction, see Ref. [20].

The results for the Fe-Ga phases show that the magnetoelasticity of the 8c site in the $D0_3$-like phase is very sensitive to the placement of the Fermi level over most of its Ga concentration range, with this sensitivity increasing along with Ga content. By studying the range of concentrations as a whole, we see that a clear pattern emerges—as we dope bcc Fe with Ga at the 8c site, a peak in magnetoelasticity emerges above the Fermi level, which increases in magnitude and moves downward in energy as more Ga is added. This closely mirrors the behavior of the lower energy peak that we observed in the minority spin of site 8c's DOS, as shown in Fig. 8. The peak associated with $Fe_{0.75}Ga_{0.25}$, which resides at around -0.01 Ry, represents an extraordinary enhancement in magnetoelasticity—nearly three times the value at the natural Fermi level and thus *six times* that of Galfenol's experimentally measured maximum.

The Fermi level dependence of the partially ordered $B2$-like phase demonstrates a similar trend to its $D0_3$-like counterpart, as we see a peak in magnetoelasticity emerge above the Fermi level at $x = 0.1$ which grows in magnitude and lowers in energy as Ga concentration increases. However, it is also clear that the maximum size of this peak is far smaller than in the $D0_3$-like case—less than half in fact.

Another contrast with the partially ordered $D0_3$-like phase is that there is no longer a correlation between the concentration dependence of the magnetoelastic peak and the peak in the minority channel of the DOS. This lack of correlation is made particularly clear by the fact that the peak in the minority DOS of $B2$-like $Fe_{0.75}Ga0.25$ resides just above the

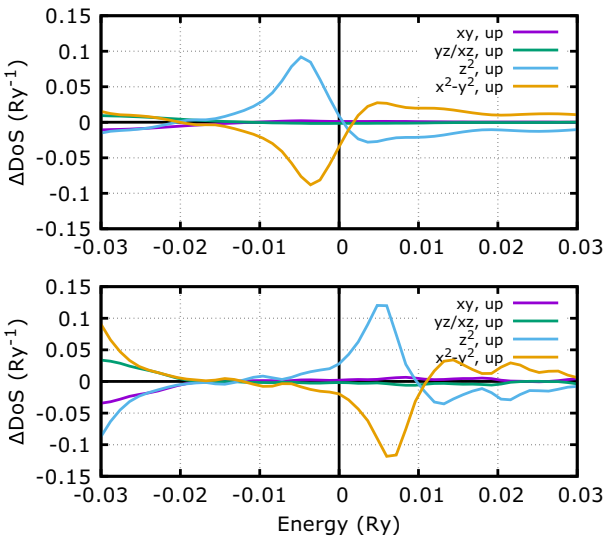

FIG. 10. The strain-induced change in the majority channel of the state-projected density of states [$\Delta\text{DOS} = \text{DOS}(\varepsilon_{zz} = 0.2\%) - \text{DOS}(\varepsilon_{zz} = 0\%)$] in $Fe_{0.75}Ga_{0.25}$. The top panel shows the 1b site of the partially ordered $B2$-like phase, and the bottom panel shows the 8c site of the $D0_3$-like phase.

Fermi level, while the magnetoelastic peak resides below. This suggests that there is an electronic mechanism beside the availability of states in the minority channel that is affecting the magnetoelasticity.

To investigate this further, we have calculated the strain-induced change in the DOS [$\Delta\text{DOS} = \text{DOS}(\varepsilon_{zz} = 0.2\%) - \text{DOS}(\varepsilon_{zz} = 0\%)$] in the majority channel of the 1b and 8c sites of the $B2$- and $D0_3$-like phases of $Fe_{0.75}Ga_{0.25}$, respectively, and plotted the results in Fig. 10. What they show is that the relatively small peaks in the majority spin channels of both phases cause a sharp redistribution of d-states around the Fermi level when the system is positively strained along the z-axis, primarily from $x^2 - y^2$ to z^2 states. From the second-order perturbation theory of the MCA detailed in Sec. II E, we can see that this represents an enhancement in the $\langle z^2|L_x|xz, yz\rangle = \sqrt{3}$ term alongside a weakening of the $\langle x^2 - y^2|L_z|xy\rangle = 2$ term, thus diminishing the MCA overall. This redistribution should therefore contribute negatively to the magnetoelasticity. However, the key difference between the $B2$- and $D0_3$-like phases in terms of these strain-induced changes is that they take place at a higher energy in the $D0_3$ phase, above the Fermi level. Thus in the $B2$-like phase, where the redistributive peak is below the Fermi level and thus energetically accessible, there is a suppression of the magnetoelasticity in comparison to the $D0_3$ phase. This explanation is further supported by the results in Fig. 9(b), which show that occupying the $D0_3$-like phase's redistributive peak by adding more electrons causes a significant decrease in magnetoelasticity.

5. Summary and discussion

In this section, we have used band-filling analysis and the tight-binding model, in conjunction with scalar relativistic calculations of state-projected DOS, to investigate the electronic origins of the magnetoelastic enhancement of $Fe_{1-x}Ga_x$'s partially ordered $B2$- and $D0_3$-like phases. We have focused solely on their 1b and 8c sites, respectively, due to the dominating influence they have on each phase's magnetoelastic concentration dependence at Ga concentrations greater than 10%.

Calculations of the DOS showed that an increase in Ga concentration leads to the emergence of a large, broad peak in the nonbonding region of the $B2$-like phase's minority spin channel, while in the $D0_3$-like phase that peak is split into two sharper peaks on either side of the Fermi level. The former result agrees well with similar calculations carried out by Khmelevska *et al.* [19], however they did not find a peak-splitting feature in the $D0_3$-like phase. Looking closely at their results, it may be the case that a greater resolution along the energy axis was required to distinguish the two peaks, especially as they are also observed in Ref. [54].

Using the Slater-Koster tight-binding model, we have provided a qualitative theory for the splitting of these peaks. While the interaction between adjacent d orbitals is equivalent in the $D0_3$- and $B2$-like configurations, the introduction of lower-symmetry interactions between the Fe's d orbitals and the Ga's p orbitals in the $D0_3$-like configuration breaks this equivalence and leads to a "symmetry-splitting."

Calculations of the magnetoelastic Fermi level dependence of the partially ordered $D0_3$-like phase showed a notable correlation with the DOS of the minority spin channel, as each curve showed the emergence of a peak that increased in magnitude and decreased in energy as Ga content was increased. Equivalent calculations in the $B2$-like phase did not show the same agreement between the electron number dependence of the magnetoelasticity and minority DOS, however. Using the second-order perturbation approximation of the MCA, we have been able to attribute the suppression of the $B2$-like phase's magnetoelasticity to a small peak in the majority DOS, which leads to a large redistribution of e_g states when the system is strained. The negative influence of a similar feature in the majority DOS was also observed by Cao *et al.* in their study of $Fe_{1-x}Ge_x$ [10].

This leads us to conclude that the dramatic magnetoelastic enhancement of $D0_3$-like $Fe_{1-x}Ga_x$ is a result of symmetry-splitting in the minority DOS leading to a large concentration of states in an optimal energy region where the majority DOS is mostly filled—with the exception of a small number of detrimental states that reside at high energies. On the other hand, while the magnetoelastic enhancement exhibited in the partially ordered $B2$-like phase is quite significant, it is ultimately limited by the fact that the peak in its minority DOS is smeared over a greater energy range due to its higher degree of symmetry and compositional disorder.

Finally, our results on the Fermi-level and Ga concentration dependence of the $D0_3$-like configuration's magnetoelasticity provide us with a qualitative theory for the experimentally measured peak [5]. While the overall peak in magnetoelasticity for a given concentration grows in magnitude as Ga is added to the system, the location of that peak is simultaneously shifted downward in energy. This leads to a critical concentration around ∼20% Ga content where the effect of the energy shift outweighs the enhancement of the peak's maximum. It is therefore possible to account for the experimentally measured peak in magnetostriction around ∼20%

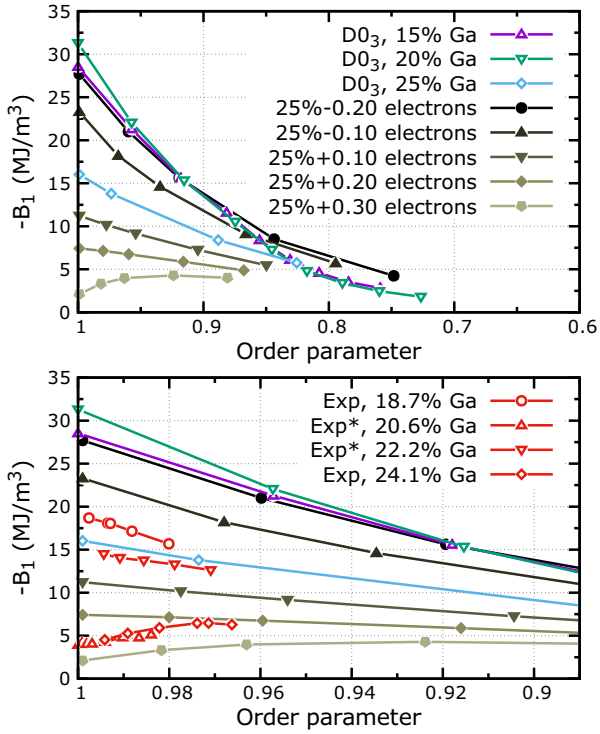

FIG. 11. B_1 as a function of magnetic order parameter m, calculated in the $B2$-like phase at Ga concentrations of 15%, 20%, and 25% (purple circles, green up-triangles, and blue down-triangles, respectively) and the $D0_3$-like phase at 20% and 25% (orange diamonds and yellow pentagons). The lower panel shows additional experimental measurements from Ref. [5], where an asterisk denotes the use of interpolation to determine experimental values of c' in the determination of B_1 (see the main text).

using only a partially ordered model of the $D0_3$-like phase, which according to our results on the ground-state compositional order in Sec. III A is the system's preferred state at $0.10 < x < 0.25$.

D. Finite-temperature magnetoelasticity

Now we will utilize DLM theory's treatment of thermally driven magnetic disorder to determine the finite-temperature magnetoelasticity of the $D0_3$-like phase at Ga concentrations of 15%, 20%, and 25%. We have plotted B_1 as a function of order parameter m in Fig. 11, where the lattice parameter is fixed at $a = 5.45$ a.u. At each concentration, our results show a monotonic decrease in magnetoelasticity as m decreases (temperature increases), roughly in line with what is expected from single ion theory [25]. It is also evident from these results that as magnetic disorder increases, there is a convergence in B_1 between different Ga concentrations. This convergence is reminiscent of the finite-temperature behavior seen in similar calculations of bcc Fe and $A2$ $Fe_{1-x}Ga_x$ in Ref. [20], which was attributed to the magnetic disorder-induced homogenization of their electronic structure.

Following from the band-filling analysis carried out at zero temperature in the previous section, we have also calculated the temperature dependence of $D0_3$-like Fe_3Ga with adjusted numbers of electrons to study how its thermal behavior could be influenced by chemical doping according to rigid band theory. The results are shown in Fig. 11. In a similar way to the different concentration curves, we find that the different curves converge between $m = 0.8$ and 0.9, therefore as more electrons are added to the system and the zero-temperature magnetoelasticity decreases, the curves no longer monotonically decrease and instead show a slight increase between $m = 1.0$ and 0.9. This is reminiscent again of the results of Ref. [20], where isovolumetric curves with small or negative zero-temperature magnetoelasticity exhibit a flat or even positive slope at $m = 1$, while curves with larger initial values quickly drop off as magnetic disorder increases.

To compare these calculations with experimental data, we have adapted the results in Ref. [5] to produce B_1 versus m, using measurements of T_C as a function Ga content found in Ref. [55] to scale the m versus T model. Without measurements of the elastic constant c' for $x = 0.206$ and 0.222 we cannot determine B_1 at these concentrations directly, so we have interpolated the published values of c' from Ref. [5]. Note that because magnetostriction is only measured up to room temperature, the experimental data represent a very small range of order parameters, $0.98 < m < 1$. Looking at the results of this procedure in the bottom panel of Fig. 11, we see that the above description of convergence at finite temperature appears to be borne out in the real system. The large $T = 0$ magnetoelasticity when $x = 0.187$ and 0.206 corresponds to the usual monotonic decrease with temperature, whereas the comparatively small $T = 0$ magnetoelasticity of $x = 0.187$ and 0.222 is enhanced by the onset of magnetic disorder.

IV. SUMMARY AND CONCLUSIONS

We have used a unified *ab initio* framework in the disordered local moment picture to study both the nature of compositional phase ordering and the temperature dependence of the magnetoelastic constant B_1 in $Fe_{1-x}Ga_x$ across a range of Ga concentrations.

The ordered phases of interest have been identified as exhibiting nonstoichiometric $B2$- and $D0_3$-like order, with a system annealed below the Curie temperature in an almost pure $D0_3$-like state. We have then opted to study the finite-temperature magnetoelastic behavior of both pure $B2$-like and pure $D0_3$-like order.

We find that, in contrast with our earlier work on pure Fe and the disordered $A2$ phase, the $B2$-like and $D0_3$-like phases exhibit a marked enhancement in the magnetoelastic constant B_1, in good agreement with experiment. In contrast to earlier works, we find that the $D0_3$ phase is not in itself detrimental to magnetostriction, but instead that the computed value of B_1 is highly sensitive to the position of the Fermi level in the material.

By studying the Fermi level dependence of the partially ordered $D0_3$-phase's magnetoelasticity, we have provided a qualitative explanation for the origin of Galfenol's magnetostrictive peak at $\sim$19% by interpreting strain-induced changes in the DOS through the second-order perturbative form of the spin-orbit coupling energy. We have found that the peak arises from the interaction between two sharp peaks in both the minority and majority DOS.

While a very recent experimental study has shown that doping $Fe_{0.83}Ga_{0.17}$ with small amounts of Cu is detrimental to magnetostriction [56], our band-filling analysis shows that enhancement could be achieved by increasing Ga content. By lowering the Fermi energy of $D0_3$ Fe_3Ga by 0.01 Ry, its magnetostriction can be increased twofold. This change can be achieved by removing ∼0.6 electrons, so applying a rigid band analysis suggests that the magnetostriction of $D0_3$-like Fe_3Ga can be increased by replacing 30% of the Ga with Cu, i.e., $Fe_3Ga_{0.7}Cu_{0.3}$. This alloy therefore warrants further investigation, but we also note that a systematic experimental and theoretical study of the magnetostriction of Fe-Ga-Cu alloys could yield valuable insight into transition-metal magnetostriction.

Finally, we note that our results confirm the inextricable link between atomic order, magnetic order, and magnetostriction in Fe-Ga alloys. We find differences in predicted structures depending on the nature of magnetic order within the material, and our results show that those structures significantly influence the magnetoelasticity of Fe-Ga. It may therefore be possible to further enhance magnetostrictive properties by fine-tuning the annealing process, for example via the application of external magnetic fields [57].

ACKNOWLEDGMENTS

The present work forms part of the PRETAMAG project, funded by the UK Engineering and Physical Sciences Research Council, Grant No. EP/M028941/1. C.D.W. is supported by a studentship within the UK Engineering and Physical Sciences Research Council-supported Centre for Doctoral Training in Modelling of Heterogeneous Systems, Grant No. EP/S022848/1.

[1] E. D. T. De Lacheisserie, in *Theory and Applications of Magnetoelasticity* (CRC Press, Boca Raton, FL, 1993), p. 430.
[2] R. Abbundi and A. Clark, IEEE Trans. Magn. **13**, 1519 (1977).
[3] A. Olabi and A. Grunwald, Mater. Design **29**, 469 (2008).
[4] S. A. Wilson, R. P. J. Jourdain, Q. Zhang, R. A. Dorey, C. R.. Bowen, M. Willander, Q. ul Wahab, S. M. Al-hilli, O. Nur, E. Quandt, C. Johannson, E. Pagounis, M. Kohl, J. Matovic, B. Samel, W. van der Wijngaart, E. W. H. Jager, Q. D. Carlsson, Z. Djinovic, M. Wegener, C. Moldovan, R. Iosub, E. Abad, M. Wendlandt, C. Rusu and K. Persson, Mater. Sci. Eng.: R **56**, 1 (2007).
[5] A. E. Clark, K. B. Hathaway, M. Wun-Fogle, J. B. Restorff, T. A. Lograsso, V. M. Keppens, G. Petculescu, and R. A. Taylor, J. Appl. Phys. **93**, 8621 (2003).
[6] A. E. Clark, J. B. Restorff, M. Wun-Fogle, D. Wu, and T. A. Lograsso, J. Appl. Phys. **103**, 07B310 (2008).
[7] R. Grössinger, R. S. Turtelli, and N. Mehmood, IOP Conf. Ser.: Mater. Sci. Eng. **60**, 012002 (2014).
[8] A. Khachaturyan and D. Viehland, Metall. Mater. Trans. A **38**, 2308 (2007).
[9] A. Khachaturyan and D. Viehland, Metall. Mater. Trans. A **38**, 2317 (2007).
[10] J. X. Cao, Y. N. Zhang, W. J. Ouyang, and R. Q. Wu, Phys. Rev. B **80**, 104414 (2009).
[11] M. Laver, C. Mudivarthi, J. R. Cullen, A. B. Flatau, W.-C. Chen, S. M. Watson, and M. Wuttig, Phys. Rev. Lett. **105**, 027202 (2010).
[12] Y. He, C. Jiang, W. Wu, B. Wang, H. Duan, H. Wang, T. Zhang, J. Wang, J. Liu, Z. Zhang, P. Stamenov, J. Coey, and H. Xu, Acta Mater. **109**, 177 (2016).
[13] Y. Du, M. Huang, S. Chang, D. L. Schlagel, T. A. Lograsso, and R. J. McQueeney, Phys. Rev. B **81**, 054432 (2010).
[14] Y. Du, M. Huang, T. A. Lograsso, and R. J. McQueeney, Phys. Rev. B **85**, 214437 (2012).
[15] R. Wu, L. Chen, and A. Freeman, J. Magn. Magn. Mater. **170**, 103 (1997).
[16] H. Wang, Y. N. Zhang, R. Q. Wu, L. Z. Sun, D. S. Xu, and Z. D. Zhang, Sci. Rep. **3**, 3521 (2013).
[17] R. Wu, J. Appl. Phys. **91**, 7358 (2002).
[18] H. Ebert, D. Ködderitzsch, and J. Minár, Rep. Prog. Phys. **74**, 096501 (2011).
[19] T. Khmelevska, S. Khmelevskyi, and P. Mohn, J. Appl. Phys. **103**, 073911 (2008).
[20] G. A. Marchant, C. E. Patrick, and J. B. Staunton, Phys. Rev. B **99**, 054415 (2019).
[21] R. J. Elliott, in *Magnetic Properties of Rare Earth Metals*, edited by R. J. Elliott (Plenum, London, 1972), p. 1.
[22] E. Callen and H. Callen, J. Phys. Chem. Solids **16**, 310 (1960).
[23] H. B. Callen and E. R. Callen, Phys. Rev. **132**, 991 (1963).
[24] A. E. Clark, B. F. DeSavage, and R. Bozorth, Phys. Rev. **138**, A216 (1965).
[25] E. Callen, J. Appl. Phys. **39**, 519 (1968).
[26] B. L. Györffy, A. J. Pindor, J. Staunton, G. M. Stocks, and H. Winter, J. Phys. F **15**, 1337 (1985).
[27] M. Born and R. Oppenheimer, Ann. Phys. **389**, 457 (1927).
[28] J. B. Staunton, S. Ostanin, S. S. A. Razee, B. L. Gyorffy, L. Szunyogh, B. Ginatempo, and E. Bruno, Phys. Rev. Lett. **93**, 257204 (2004).
[29] J. B. Staunton, L. Szunyogh, A. Buruzs, B. L. Gyorffy, S. Ostanin, and L. Udvardi, Phys. Rev. B **74**, 144411 (2006).
[30] M. Matsumoto, R. Banerjee, and J. B. Staunton, Phys. Rev. B **90**, 054421 (2014).
[31] C. E. Patrick, S. Kumar, G. Balakrishnan, R. S. Edwards, M. R. Lees, L. Petit, and J. B. Staunton, Phys. Rev. Lett. **120**, 097202 (2018).
[32] B. L. Gyorffy and G. M. Stocks, Phys. Rev. Lett. **50**, 374 (1983).
[33] J. B. Staunton, D. D. Johnson, and F. J. Pinski, Phys. Rev. B **50**, 1450 (1994).
[34] S. N. Khan, J. B. Staunton, and G. M. Stocks, Phys. Rev. B **93**, 054206 (2016).
[35] F. Ducastelle, *Order and Phase Stability in Alloys* (North-Holland, New York, 1991).
[36] L.-Q. Chen and A. Khachaturyan, Scr. Metall. Mater. **25**, 61 (1991).

[37] D. P. Landau and K. Binder, *A Guide to Monte Carlo Simulations in Statistical Physics*, 4th ed. (Cambridge University Press, Cambridge, 2014).
[38] L. J. Santodonato, P. K. Liaw, R. R. Unocic, H. Bei, and J. R. Morris, Nat. Commun. **9**, 4520 (2018).
[39] P. Soven, Phys. Rev. **156**, 809 (1967).
[40] G. M. Stocks, W. M. Temmerman, and B. L. Gyorffy, Phys. Rev. Lett. **41**, 339 (1978).
[41] A. Pindor, W. Temmerman, and B. Gyorffy, J. Phys. F **13**, 1627 (1983).
[42] C. Kittel, Rev. Mod. Phys. **21**, 541 (1949).
[43] A. E. Clark, J. B. Restorff, M. Wun-Fogle, T. A. Lograsso, and D. L. Schlagel, IEEE Trans. Magn. **36**, 3238 (2000).
[44] X. Wang, R. Wu, D.-S. Wang, and A. J. Freeman, Phys. Rev. B **54**, 61 (1996).
[45] D. S. Wang, R. Wu, and A. J. Freeman, Phys. Rev. B **47**, 14932 (1993).
[46] R. Wu, L. Chen, A. Shick, and A. Freeman, J. Magn. Magn. Mater. **177-181**, 1216 (1998).
[47] R. Wu and A. Freeman, J. Magn. Magn. Mater. **200**, 498 (1999).
[48] A. Kumagai, A. Fujita, K. Fukamichi, K. Oikawa, R. Kainuma, and K. Ishida, J. Magn. Magn. Mater. **272**, 2060 (2004).
[49] H. Wang, Y. Zhang, T. Yang, Z. Zhang, L. Sun, and R. Wu, Appl. Phys. Lett. **97**, 262505 (2010).
[50] R. Dunlap, J. McGraw, and S. Farrell, J. Magn. Magn. Mater. **305**, 315 (2006).
[51] J. C. Slater and G. F. Koster, Phys. Rev. **94**, 1498 (1954).
[52] Y. Zhang, J. Cao and R. Wu, Appl. Phys. Lett. **96**, 062508 (2010).
[53] J. Franse, R. Winkel, R. Veen, and G. D. Vries, Physica **33**, 475 (1967).
[54] C. Paduani and C. Bormio-Nunes, J. Appl. Phys. **109**, 033705 (2011).
[55] J. Borrego, J. Blazquez, C. Conde, A. Conde, and S. Roth, Intermetallics **15**, 193 (2007).
[56] X. Zhao, X. Tian, Z.-Q. Yao, L.-J. Zhao, R. Wang, and J. Yan, Rare Met. 1 (2020).
[57] N. Maât, I. McDonald, R. Barua, B. Lejeune, X. Zhang, G. Stephen, A. Fisher, D. Heiman, I. Soldatov, R. Schäfer *et al.*, Acta Mater. **196**, 776 (2020).